



Density functional theory study on the effect of Cu- and Na-substituted layers on spin-dependent transport and TMR in the Fe/ZnO/Fe MTJ

Masoud Ansarino¹

Received: 28 July 2019 / Accepted: 24 August 2019 / Published online: 31 August 2019
© The Author(s) 2019

Abstract

Using density functional theory, effects of Na- and Cu-substituted layers on the spin-dependent electronic transport properties of Fe/ZnO/Fe magnetic tunnel junction based on zinc oxide barrier tunnel, with rock-salt crystalline structure, have been studied. In zero-bias voltage, conductance and tunneling magneto-resistance (TMR) ratio of structures are calculated. It is showed that substituted layers in the pristine junction greatly affect conductance and TMR ratio of this junction. The results indicated that Cu-substituted layer with reducing conductance of pristine structure in the antiparallel alignment configuration, and increasing its conductance in the parallel alignment, leads to a large TMR ratio, up to 1800%. Due to the large conductance of pristine and Cu-substituted devices in the parallel alignment, these structures would be very beneficial for experimental applications that require the spin-polarized current.

Keywords Rock-salt ZnO · Spintronics · MTJ · TMR · Nanostructure

Introduction

One of the most important topics in spintronics is the study of conductance and TMR phenomenon in the magnetic tunnel junction (MTJ) devices. In a MTJ device, two ferromagnetic electrodes are separated by a non-magnetic insulator or semiconductor, known as tunnel barrier or separator, with a few nanometers thickness. Electron transport in MTJs is spin-dependent and carried out via quantum tunneling. The electrical resistance of MTJs differs in two settings, when the magnetizations of left and right electrodes are parallel and when they are antiparallel, resulting in the TMR phenomenon. Under zero-bias voltage, the TMR ratio is conventionally defined as

$$\text{TMR} = \frac{G_{\text{PA}} - G_{\text{APA}}}{G_{\text{APA}}} \quad (1)$$

where G_{PA} (G_{APA}) is the conductance of the MTJ in parallel (antiparallel) alignment of magnetizations of the electrodes.

Furthermore, at a finite bias, $\text{TMR} = (I_{\text{PA}} - I_{\text{APA}})/I_{\text{APA}}$. In this equation, I_{AP} (I_{APA}) is the electrical current through the device in parallel (antiparallel) alignment of the electrode magnetizations. The type and thickness of barrier layer and the applied bias voltage are important parameters that can affect TMR ratio. The thickness dependence of magneto-resistance and TMR in MTJs has been previously investigated [1–4]. The other factor that influences the amount and sign of TMR ratio is structural asymmetry in MTJs. Heiliger et al. [5, 6] reported that in the asymmetric junction, independent of the voltage used, the I_{APA} is higher than I_{PA} , which results in a negative TMR ratio. Also, Waldron et al. [7, 8] reported that the zero-bias TMR in MgO-based MTJs is substantially reduced by oxidization of the junction interface. This oxidized junction can also be considered as a structural asymmetry.

The crystal structures shared by zinc oxide (ZnO) are wurtzite hexagonal, zinc blend, and rock salt [9]. It is accepted that pure ZnO is a non-magnetic material [10, 11]. In the past decade, novel functionalities of ZnO with wurtzite crystalline structure in the electronic, optoelectronic, and spintronic applications have been extensively studied, theoretically and experimentally [12–16].

Recently, ZnO with rock-salt crystalline structure is taken into consideration because of its possible applications in

✉ Masoud Ansarino
M_Ansarino@Azad.Ac.Ir

¹ Department of Physics, South Tehran Branch, Islamic Azad University, Tehran, Iran

spintronics. Owing to its wide band gap (2.45 eV) [17], it can be considered as a semiconductor material for non-magnetic tunnel barrier in the MTJ devices. Spin-dependent electronic transport properties of rock-salt-type ZnO-based MTJs have been investigated in some studies before [18, 19].

In this paper, the geometrical asymmetry effects on the zero-bias spin-dependent electronic transport properties, conductance, and TMR ratio in a MTJ based on ZnO with rock-salt structure were studied. The Fe(001)/ZnO(001)/Fe(001) junction with four ZnO barrier layer thicknesses is used as a pristine structure (PS). The elements sodium (Na) and copper (Cu) are used to make geometrically asymmetric substituted structures (SS). The significant influence on the conductance and TMR ratio of the pristine symmetric device is the main reason for choosing these two elements, which have closest electronic structures to Mg and Zn. The main goal is to find new materials that have a significant impact on the conductance and TMR of this MTJ. Similar calculations for other elements as substituted material were reported [19].

Computational details

First-principle calculations based on spin-polarized density functional theory (DFT) method are employed to determine the electronic transport properties of these MTJs. For our DFT analysis, we use the software package QuantumATK [20] with the PAW pseudopotentials within the gradient approximation (GGA) for the PBE exchange–correlation functional [21]. For calculating the spin-dependent

electronic transport properties, QuantumATK uses the non-equilibrium Green’s function formalism. Following the Monkhorst–Pack scheme [22], the k -point mesh for energy integration within the irreducible region of the Brillouin zone (BZ) is chosen as $7 \times 7 \times 100$ for transport calculations. The energy cutoff for separating the core electrons from the valence electrons is set equal to 200 Hartree. Structural optimizations are carried out until atomic force reached below 0.01 eV/Å. Self-consistency is achieved when the change in the total energy between cycles of the SCF procedure is reduced to less than 10^{-6} eV.

In pristine structure (PS), two semi-infinite Fe electrodes (in their [001] direction) are attached to the rock-salt ZnO (001) barrier with four-monolayer (4-ML) thickness (Fig. 1). The resulting two-probe device is laterally periodic such that the electrodes are fully three dimensional in a half plane. Along the Z -axis (transmission direction), the two electrodes are semi-infinite. The transverse lattice constants of the device (a and b) are set equal to the experimental constant of bulk Fe, which is 2.866 Å.

The structural force optimization calculations are carried out to obtain the optimized central region length, L , as shown in Fig. 1. Three layers of the electrodes at either side of the junction are taken as part of the central region. This is done to eliminate the effects of the barrier region on the electronic structure of the electrodes, enabling a semi-infinite behavior. In the direction parallel to the junction’s interface (X – Y plane), periodic boundary conditions are imposed.

In order to make two asymmetric SSs, the first Zn atom from left side of the barrier is replaced with one of the two

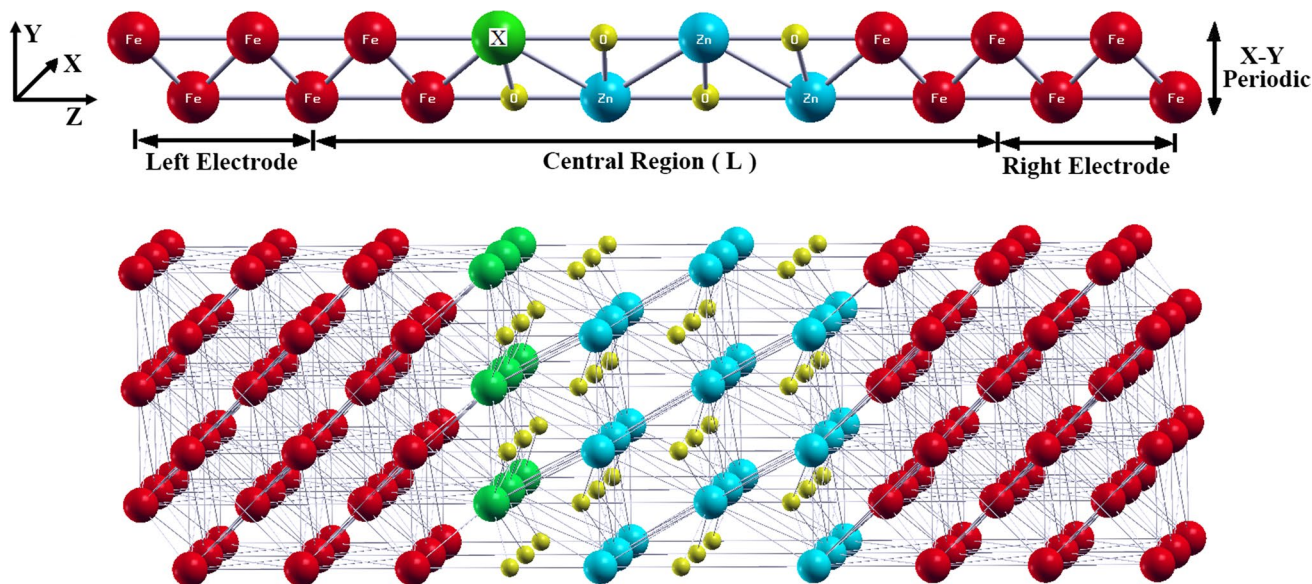


Fig. 1 (Colored) Atomic structure of MTJs with a 4-ML barrier sandwiched between two Fe electrodes. The symbol \boxtimes stands for atomic elements Zn in PS and Na and Cu in substituted structures. Top and

bottom panels show the unit cell, and the same cell after nine repetitions, respectively. “ L ” is the length of central region of the device

Table 1 Calculated values of the optimized central region lengths

	PS	Na-SS	Cu-SS
L (Å)	13.71	14.45	14.46

Table 2 Calculated atomic distances (in angstrom) at the left and right interfaces of barrier with electrodes

	Left		Right	
	Fe-X	Fe-O	Fe-Zn	Fe-O
PS	2.652	2.082	2.652	2.082
Na-SS	3.178	1.706	2.591	2.240
Cu-SS	2.469	2.081	3.194	1.951

The symbol X stands for atomic elements Zn in PS and Na and Cu in substituted structures

Na and Cu atoms, separately. The unit cell of these MTJs is shown in Fig. 1, where the symbol \boxtimes stands for atomic elements Zn in PS and one of the two Na and Cu elements in SSs.

The following calculations are performed in our analysis: (1) structural force optimization; (2) Mulliken population per spin channel for each atom; (3) density of states (DOS) of structures; (4) energy and k -point-dependent transmission spectrum; and (5) conductance and TMR ratio of the structures;

Results and discussion

The structural optimization of the central region is carried out by fixing the transverse (X - Y plane) lattice constants of the device at the experimental lattice constant of bulk Fe, and allowing the length “ L ” to vary. The above-mentioned optimization process is repeated separately for all three

structures, and the optimized central region lengths are given in Table 1. As can be seen from Table 1, substituted layer causes the L values of both SSs to be greater than that of the PS. Calculated Fe-O and Fe-X (X =Zn, Na, Cu) junction lengths at the left and right interfaces of barrier with electrodes are given in Table 2. From these values, it can be concluded that all structures are oxygen-terminated.

To independently adjust the electrodes’ magnetization in the MTJs, the tunnel barrier must be able to prevent the permeation of magnetization of the electrodes to each other. To this end and to ensure that all atoms in the considered MTJs are correctly spin polarized in our calculations, Mulliken population per spin channel is calculated for each atom. Mulliken population of atom “ i ” is calculated using the relation $M_i = \sum_{j \in i} \sum_{jm} D_{jm} S_{mj}$, where D and S are the density and overlap matrices, respectively [19]. The sum is taken over all orbitals in the considered atom. The results of this calculation for atoms in the central region of the PS and Cu-SS in APA and PA configurations are summarized in Tables 3 and 4, respectively. The difference between spin-up and spin-down populations determines the polarization of each atom, and multiplying this polarization by Bohr magneton gives the magnetic momentum of that atom. From these tables, it can be verified that while Fe atoms are correctly spin polarized and the atoms next to the interface (on both left and right sides) are slightly affected by magnetization of Fe atoms, the remnant atoms in the barrier far from the interface are un-polarized. Therefore, it can be said that the barrier region is well prevented from penetrating the magnetizations of the two electrodes. Another important point is that the Fe atoms in the left and right electrodes in the PS have completely symmetric spin polarizations, but this symmetry is not present in the SSs. This can affect the spin-dependent transport in these asymmetric devices. The behavior of Mulliken population in the Na-SS is similar to the results shown in Table 4.

Table 3 Mulliken atomic populations for atoms in the central region in the PS

	Fe	Fe	Fe	Zn	O	O	Zn	Zn	O	O	Zn	Fe	Fe	Fe
Spin-up	5.13	5.20	5.45	5.59	3.39	3.38	5.61	5.60	3.38	3.32	5.66	2.60	2.82	2.88
Spin-down	2.88	2.82	2.60	5.66	3.32	3.38	5.60	5.61	3.38	3.39	5.59	5.45	5.20	5.13
Spin-up	5.13	5.20	5.45	5.59	3.39	3.38	5.61	5.61	3.38	3.39	5.59	5.45	5.20	5.13
Spin-down	2.88	2.82	2.60	5.65	3.33	3.38	5.60	5.60	3.38	3.33	5.65	2.60	2.82	2.88

The first and second rows show the spin populations of APAC and the third and fourth rows PACs. All numbers are rounded

Table 4 Mulliken atomic populations for atoms in the central region in the Cu-SS

	Fe	Fe	Fe	Cu	O	Zn	O	Zn	O	Zn	O	Fe	Fe	Fe
Spin-up	5.07	5.19	5.41	5.34	3.36	5.62	3.37	5.63	3.36	5.63	3.33	2.37	2.87	2.95
Spin-down	2.93	2.89	2.59	5.21	3.23	5.60	3.37	5.64	3.37	5.62	3.38	5.48	5.16	5.05
Spin-up	5.07	5.19	5.41	5.34	3.36	5.62	3.37	5.64	3.37	5.62	3.38	5.48	5.16	5.05
Spin-down	2.93	2.89	2.59	5.21	3.23	5.61	3.37	5.63	3.36	5.63	3.33	2.37	2.87	2.95

In order to explain the effect of Na- and Cu-substituted layers on the magneto-resistive behavior of the junctions, the total electronic DOS of junctions are calculated for PA and APACs. The results for the barrier region are plotted in Fig. 2. In all figures of this article, zero of the energy is shifted to the Fermi level. As can be seen from this figure, substituted layer causes an increase in the DOS of both SSs compared to PS, for APA and PA configurations at Fermi level. In the APA configuration (top row), for the case of Na-SS, the increase is significantly greater than that of Cu-SS. Meanwhile, in PAC (bottom row), this increase is much greater for Cu-SS.

In the next step, the spin-dependent transport properties of these three MTJs by calculating the spin-dependent transmission spectrum of the electrons through the barrier tunnel region as a function of the energy of the electrons have been studied. Using Landauer formalism, the transmission through the barrier as a function of total energy of the electrons is extracted using the NEGF formalism [23]:

$$T(E) = \text{Tr}[\Gamma_L G^r \Gamma_R G^a] \quad (2)$$

where G^r (G^a) is the retarded (advanced) Green's function and Γ_L (Γ_R) is the self-energy of coupling function to the left (right) electrode. Figure 3 shows the energy-dependent transmission spectrum of these structures for both configurations. The following results can be extracted from this figure:

(1) In APAC, the symmetry between up- and down-spin channel's transmission for PS, which is one of the spintronic

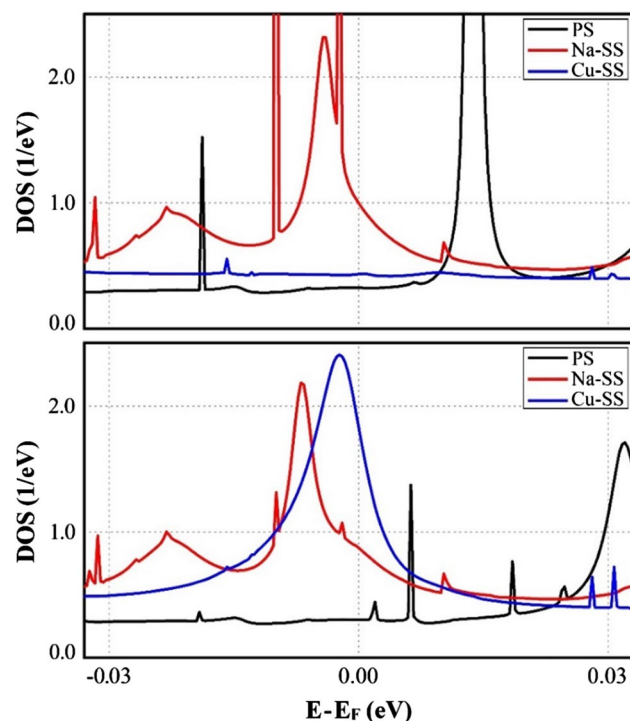


Fig. 2 (Colored) DOS of barrier region for APA (top) and PAC (bottom)

properties of MTJs with a symmetric structure, is lost in the two SSs; (2) for both APA and PACs, compared to PS, Na-SS's up- and down-spin channel transmission (left column) has severely reduced for all energies, which results in a reduction in the total transmission (right column) of this SS compared to PS. This reduction for PAC is much greater than that of the other configuration, especially at the Fermi level; (3) for the Cu-SS, transmission of spin-down channel in the Fermi level has a significant decrease in both configurations compared to that of PS. Meanwhile, in the spin-up channel, transmission of both configurations is increased; however, this increase for PAC is much greater compared to their APAC. Which results in APAC, compared to PS, total transmission in the Fermi level has not changed much, while for PAC increased.

Given the changes in the transmission spectrum of two SSs, it can be predicted that their conductance in both configurations will be reduced compared to the PS, and only in the PAC of the Cu-SS, the conductance will be increased.

The conductance of a device is calculated using the relation [24]:

$$G = \frac{e^2}{h} \sum_{k_{\parallel}} [T(k_{\parallel})]_{E_F} \quad (3)$$

where e and h are the electron's charge and Planck's constant, respectively, and $[T(k_{\parallel})]_{E_F}$ is the k_{\parallel} -dependent transmission at the Fermi energy. The k_{\parallel} represents the wave vector component in the first two-dimensional BZ, perpendicular to the transport direction (X - Y plane).

To calculate the MTJ's conductance from Eq. 3, it is necessary to study the transmission spectrum at the Fermi energy as a function of the k_{\parallel} (k_x and k_y). The results of these k -resolved calculations of the MTJs within in two-dimensional BZ perpendicular to the transport direction in the APA and PA configurations are plotted in Fig. 4. The important results of this figure are:

(A) In the APA configuration (left column), the substituted layer causes the transmission peaks of the SSs to be closer to the Γ point and concentrated around it, in comparison with the PS. This concentrating is much more intense for Cu-SS. The height of the peaks in Cu-SS is approximately equal to PS, and for the case of Na-SS, these peaks are more than one order of magnitude smaller for PS. In the PS, the peaks are very sharp and their number is low. Meanwhile, in SSs, the peaks have become very wide. In other words, relative to PS, the transmission spectrum of substituted structures shows nonzero and calculable values in a wider region of BZ; (B) in the PA configuration (right column), the substituted layer causes the transmission peaks of the SSs to be far from the Γ point and more dispersed. The height of these peaks in Na-SS is more than one order of magnitude

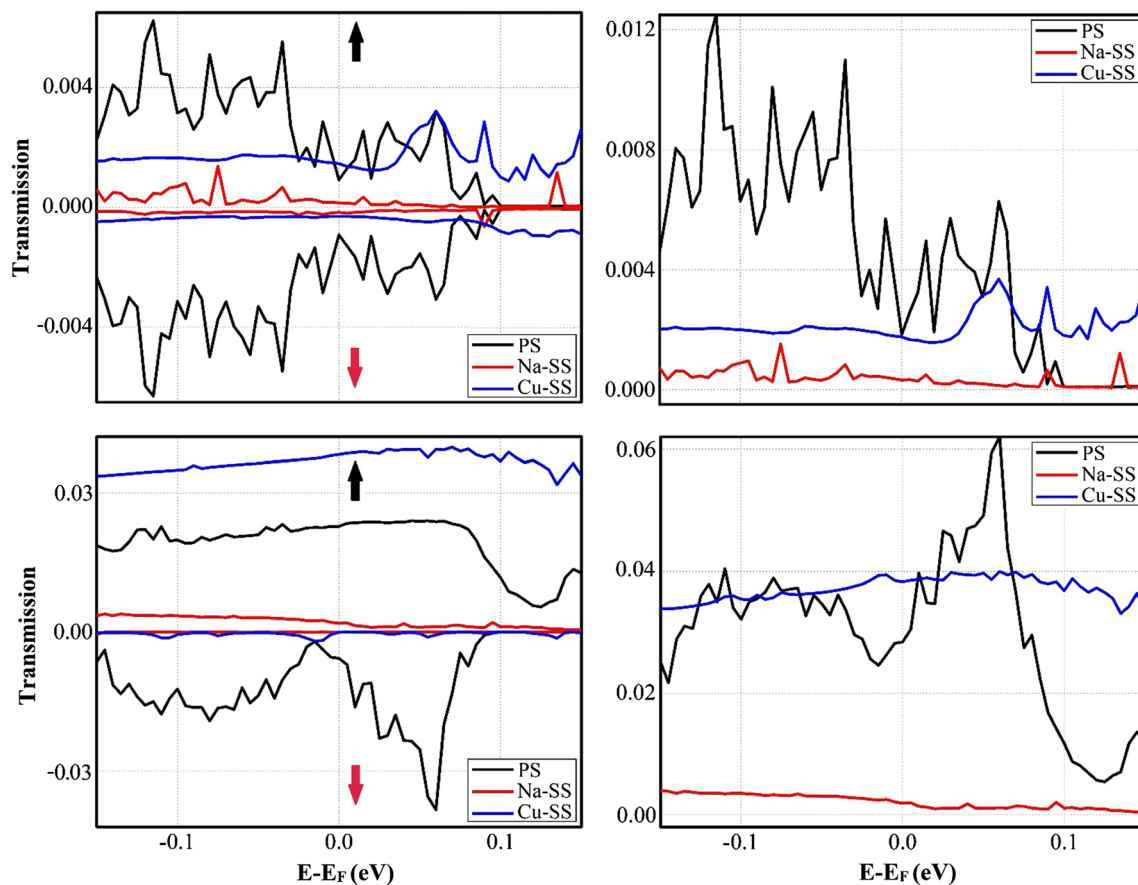


Fig. 3 (Colored) Energy-dependent transmission spectrum for all structures. Top and bottom rows for APAC and PAC, respectively. Left and right columns for spin-resolved and total transmission spectra. The black and red arrows represent up- and down-spin channels, respectively

reduced in comparison with the PS and has become broader than those for PS. In the case of Cu-SS, the peaks have not changed sensible compared to the PS, but the width of these peaks has increased significantly.

Given that the conductance is calculated by summing the $T(k_{\parallel})$, the above results have important effect on the conductance of both configurations of MTJs.

Figure 5 shows the conductance of PS and two substituted structures calculated using the relation in Eq. 3 for both APA and PACs. This figure confirms the predictions based on $T(E)$ and $T(k_{\parallel})$ calculations. It can be seen that in APA configuration, conductance of both SSs is reduced relative to PS. This reduction for Na-SS is more than that for Cu-SS. In PAC, conductance of Na-SS dropped sharply compared to PS and has been a little increase for Cu-SS relative to it.

The fact that substituting a Cu layer in the ZnO-based MTJ leads to a decrease in conductance in the APA configuration, and an increase in conductance in PAC of that MTJ, would be very beneficial for experimental applications that require the spin-polarized current.

Using the calculated values for G_{APA} and G_{PA} with the aid of Eq. 1, the zero-bias TMR ratio is calculated for all three

structures and the results are summarized in Table 5. Three important results are: (1) Cu-substituted layer in the PS, with increasing in conductance of PA configuration, and decreasing in conductance of PAC in that MTJ, leads to a threefold increase in the TMR ratio of the device; (2) in the case of Na, substituted layer in the PS, with decreasing in conductance of both configurations, leads to a decrease in TMR ratio in PS, and (3) geometrical asymmetry in these two substituted structures does not lead to a negative TMR ratio, while there are some reports that the geometric asymmetry in the MTJs can cause TMR ratio to be negative [5, 6, 20].

Conclusion

First-principle calculations, based on spin-polarized DFT and NEGF methods, are applied to study effect of Na- and Cu-substituted layers on spin-dependent electron transport properties, conductance, and TMR ratio of Fe(001)/ZnO(001)/Fe(001) magnetic tunnel junction based on zinc oxide barrier tunnel with rock-salt crystalline structure. It is shown that substituting the layers of Na and Cu in the

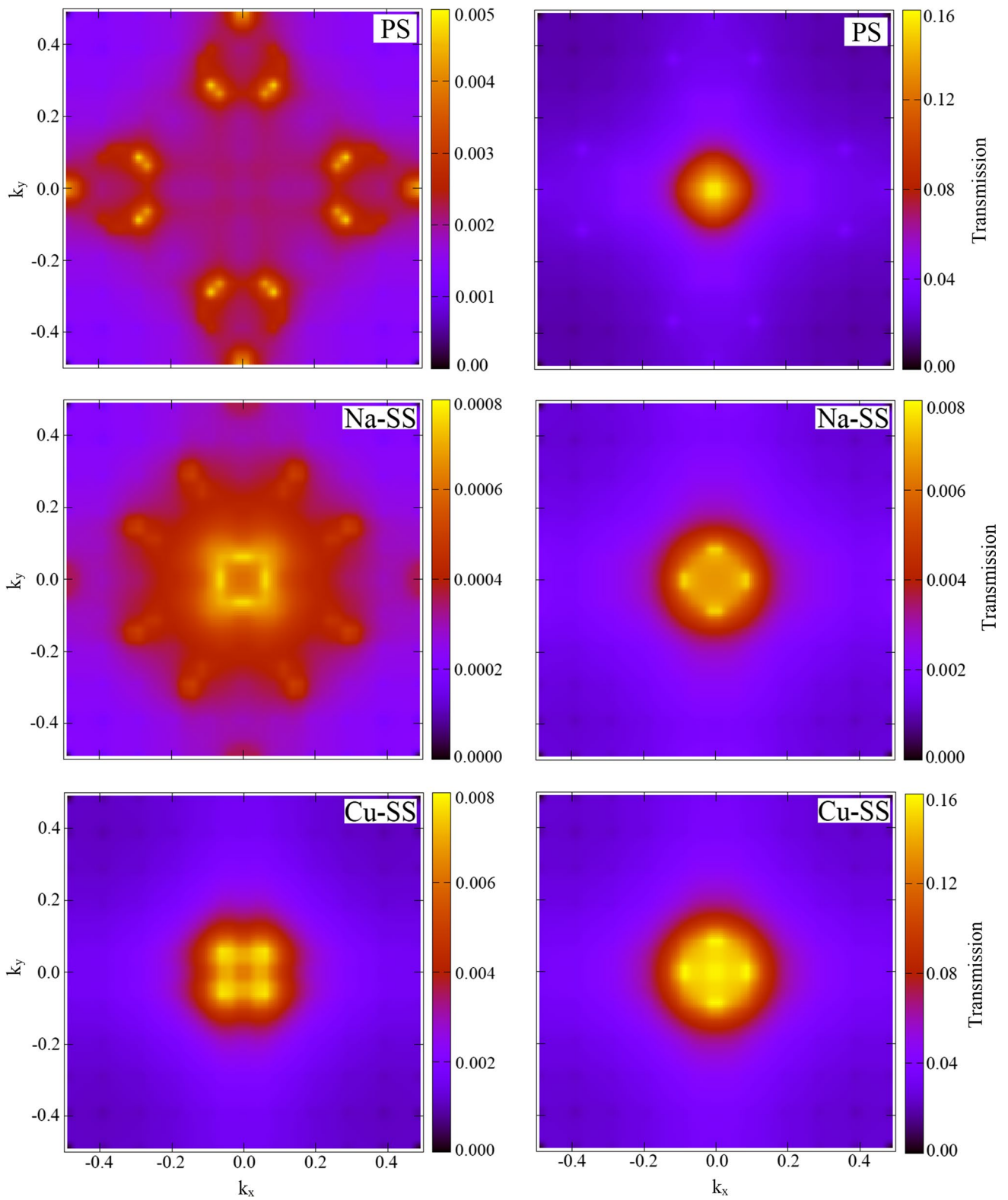


Fig. 4 (Colored) k -resolved transmission spectrum of the MTJs within in two-dimensional Brillouin zone, perpendicular to the transport direction. APAC (left column) and PAC (right column)

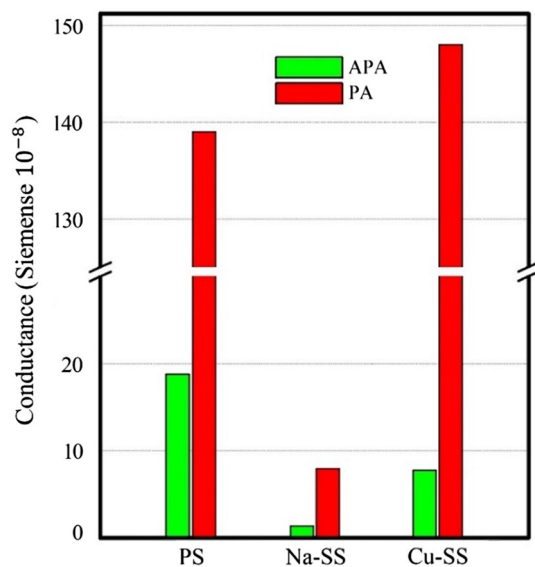


Fig. 5 (Colored) Conductance of PA and APACs for pristine and substituted structures

Table 5 Calculated values of the TMR ratio in percent

	PS	Na-SS	Cu-SS
TMR	639.36	473.91	1807.22

The first and second rows show the spin populations of APAC and the third and fourth rows PACs

pristine Fe/ZnO/Fe junction greatly affects DOS, $T(E)$, $T(k_{\parallel})$, conductance, and TMR ratio, without changing its sign, of this device. Using Mulliken population per spin channel calculations, it is observed that in all three MTJs, the barrier region is well prevented from penetrating the magnetizations of the two electrodes. It is also showed that Cu-substituted layer with reducing conductance of pristine structure in the APA configuration, and increasing its conductance in the PAC, leads to a significant increase in the TMR ratio of Cu-SS compared to PS. But in the case of Na-SS, this ratio has a small decrease relative to PS. Due to the large conductance of the PS and Cu-SS in the PAC, these structures can be used to generate electric current with pure spin for experimental purposes.

Acknowledgements Author thanks Khadijeh Khalili, Technical University of Denmark, for valuable and constructive discussion and comments during calculations and preparation of this manuscript. This research did not receive any specific grant from funding agencies in the public, commercial, or not-for-profit sectors.

Open Access This article is distributed under the terms of the Creative Commons Attribution 4.0 International License (<http://creativecommons.org/licenses/by/4.0/>), which permits unrestricted use, distribution, and reproduction in any medium, provided you give appropriate

credit to the original author(s) and the source, provide a link to the Creative Commons license, and indicate if changes were made.

References

1. Mathon, J., Umerski, A.: Theory of tunneling magnetoresistance of an epitaxial Fe/MgO/Fe (001) junction. *Phys. Rev. B* **63**, 220403 (2001)
2. Parkin, S.P., Kaiser, C., Panchula, A.: Giant tunnelling magnetoresistance at room temperature with MgO (100) tunnel barriers. *Nat. Mater. (Lett.)* **3**, 862 (2004)
3. Ikeda, S., Hayakawa, J., Ashizawa, Y.: Tunnel magnetoresistance of 604% at 300 K by suppression of Ta diffusion in Co Fe B/Mg O/Co Fe B pseudo-spin-valves annealed at high temperature. *Appl. Phys. Lett.* **93**, 082508 (2008)
4. Wang, T.X., Li, Y., Lee, K.J.: Influence of interface state in Fe/MgO/Fe magnetic tunnel junction system: C modified interfaces—a first principle study. *J. Appl. Phys.* **109**, 083714 (2011)
5. Heiliger, C., Zahn, P., Yu, B.: Influence of the interface structure on the bias dependence of tunneling magnetoresistance. *Phys. Rev. B* **72**, 180406 (2005)
6. Heiliger, C., Zahn, P., Yu, B.: Interface structure and bias dependence of Fe/MgO/Fe tunnel junctions: Ab initio calculations. *Phys. Rev. B* **73**, 214441 (2006)
7. Waldron, D., Timoshevskii, V., Hu, Y.: First principles modeling of tunnel magnetoresistance of Fe/MgO/Fe trilayers. *PRL* **97**, 226802 (2006)
8. Waldron, D., Liu, L., Guo, H.: Ab initio simulation of magnetic tunnel junctions. *Nanotechnology* **18**, 424026 (2007)
9. Ozgur, U., Alivov, Ya.I., Liu, C.: A comprehensive review of ZnO materials and devices. *J. Appl. Phys.* **98**, 041301 (2005)
10. Ren, J., Zhang, H., Cheng, X.: Electronic and magnetic properties of all 3d transition-metal-doped ZnO monolayers. *Int. J. Quantum Chem.* **113**, 2243 (2013)
11. Zhang, M., Shi, X., Wang, X.: Transition Metal Adsorbed-Doped ZnO Monolayer: 2D Dilute Magnetic Semiconductor, Magnetic Mechanism, and Beyond 2D. *ACS Omega* **2**, 1192 (2017)
12. Wang, Y., Wang, B., Zhang, Q.: Tunable electronic properties of ZnO nanowires and nanotubes under a transverse electric field. *J. Appl. Phys.* **113**, 034301 (2013)
13. Tang, S., Tang, N., Meng, X.: Enhanced power efficiency of ZnO based organic/inorganic solar cells by surface modification. *Physica E* **83**, 398 (2016)
14. Huang, H., Zhao, Q., Hong, K.: Optical and electrical properties of N-doped ZnO heterojunction photodiode. *Physica E* **57**, 113 (2014)
15. Sohn, J.I., Choi, S.S., Morris, S.M.: Novel nonvolatile memory with multibit storage based on a ZnO nanowire transistor. *Nano Lett.* **10**, 4316 (2010)
16. Choi, S.H., Jang, B.H., Park, J.S.: Low voltage operating field effect transistors with composite In₂O₃-ZnO-ZnGa₂O₄ nanofiber network as active channel layer. *ACS Nano* **8**, 2318 (2014)
17. Rossler, U., da Silva, E.C.F.: *Semiconductors*, Subvolume D. Springer, Berlin (2011)
18. Uehara, Y., Furuya, A., Sunaga, K., Magn, J.: Magnetic Tunnel Junctions with Low Resistance-area product of 0.5 $\Omega\mu\text{m}^2$. *Soc. Jpn* **34**, 311 (2010)
19. Ansarino, M., Moghaddam, H.M.: The dependence of TMR on the barrier thickness, bias voltage and asymmetry in Fe/ZnO/Fe MTJs: a DFT study. *Phys. E Low-dimens.* **107**, 80 (2019)
20. Distributed by QuantumWise Company, Copenhagen, Denmark. <https://www.synopsys.com/silicon/quantumatk.html>
21. Perdew, J.P., Burk, K., Ernzerhof, M.: Generalized gradient approximation made simple. *Phys. Rev. Lett.* **77**, 3865 (1996)
22. Monkhorst, H.J., Pack, J.D.: Special points for Brillouin-zone integrations. *Phys. Rev. B* **13**, 5188 (1976)

23. Datta, S.: *Electronic Transport in Mesoscopic*. Cambridge University Press, Cambridge (1995)
24. Landauer, R.: Spatial variation of currents and fields due to localized scatterers. *IBM J. Res. Dev.* **1**, 223 (1957)

Publisher's Note Springer Nature remains neutral with regard to jurisdictional claims in published maps and institutional affiliations.